ETH ZÜRICH

DOCTORAL THESIS

Same-sign dileptons as a search tool at CMS

Author:
Marc Dünser

Supervisor:
Prof. Dr. Rainer Wallny

A thesis submitted in fulfilment of the requirements
for the degree of Doctor of Science

in the

Institute for Particle Physics
D-PHYS

December 2014

Declaration of Authorship

I, Marc Dünser, declare that this thesis titled, 'Same-sign dileptons as a search tool at CMS' and the work presented in it are my own. I confirm that:

- This work was done wholly or mainly while in candidature for a research degree at this University.
- Where any part of this thesis has previously been submitted for a degree or any other qualification at this University or any other institution, this has been clearly stated.
- Where I have consulted the published work of others, this is always clearly attributed.
- Where I have quoted from the work of others, the source is always given. With the exception of such quotations, this thesis is entirely my own work.
- I have acknowledged all main sources of help.
- Where the thesis is based on work done by myself jointly with others, I have made clear exactly what was done by others and what I have contributed myself.

Signed: _____

Date: _____

"Thanks to my solid academic training, today I can write hundreds of words on virtually any topic without possessing a shred of information, which is how I got a good job in journalism."

Dave Barry

ETH ZÜRICH

Abstract

Faculty Name
D-PHYS

Doctor of Science

Same-sign dileptons as a search tool at CMS

by Marc Dünser

The Thesis Abstract is written here (and usually kept to just this page). The page is kept centered vertically so can expand into the blank space above the title too…

Acknowledgements

The acknowledgements and the people to thank go here, don't forget to include your project advisor…

For/Dedicated to/To my...

Contents

Chapter 1

Introduction

The construction of the Large Hadron Collider (LHC) and its experiments at CERN in Geneva over the few last decades has been just the last step in a long and successful history of particle accelerators that started roughly 100 years ago. Just as the first specimens of its kind, the LHC serves – first and foremost – the purpose of fundamental research. It has been conceived in order to answer some of the most fundamental questions of modern day physics, such as *'how do particles acquire mass?'* or *'what is dark matter?'*. Despite the purely scientific origin of these questions and the improbability of any 'practical' application from any possible answer to them, it is important to note that fundamental research in general and the research at the LHC in particular do serve a greater and more applicable purpose.

The invention of the world wide web and HTML FIXME(CITE), early developments on touch screens, research on medical physics with high-power magnet systems as well as medical imaging and the use of high energy ion beams for tumor treatment are only a few examples of the direct consequences on daily life which fundamental research on particle physics entails.

This thesis is dedicated almost exclusively to data analysis of high-energy particle collisions which took place in the CMS experiment at the LHC. By looking at such collisions, the aforementioned question about the origin of mass has already been answered FIXME(CITE) with the discovery of the Higgs boson in 2012 by both the CMS and ATLAS collaborations. The second question, however, remains unanswered and the work presented in the following is largely devoted to a search for particles which could provide physicists with a suitable candidate for a dark-matter particle.

Chapter 2 describes the fundamentals of particle physics from a theoretical standpoint, Chapter FIXME will provide on overview of the CMS experiment. Chapters FIXME to FIXME will then describe the search for new physics etc. blabla.

Chapter 2

Theory

In order to interpret any experimental result, it is of paramount importance to understand the underlying model governing the physical processes in question. Modern physics knows a large number of rather successful theories all dedicated to describing different mass and energy scales. An example is the theory of classical mechanics, which manages to describe the physics of 'daily life' very well. However, it breaks down when velocities approach the speed of light and has to be incorporated into a broader theory, namely that of relativity.

This specific example already suggests that different physical theories are valid only in a certain energy range and describe only a certain 'type'[1] of physical process. This fact is also true for the case of particle physics. The relevant theory is called the *'Standard Model'* and will be described hereafter. Further into the chapter, a short description of the pitfalls of the standard model will be given with some explanation on possible solutions.

2.1 The Standard Model

The Standard Model (SM) of particle physics provides the theoretical framework that describes all fundamental particles and the forces that act between them, with the one exception of gravity. Despite a few drawbacks that will be described later (see Section 2.1.3) it has been an overwhelmingly successful theory, capable of describing experimental data with a precision that is simply outstanding.

[1] In this particular example electromagnetic interactions are – for instance – not described at all.

Chapter 3

Experimental Setup

All data analysed in this thesis was recorded with the CMS experiment at the Large Hadron Collider (LHC) at the European Organization for Nuclear Research (CERN) near Geneva, Switzerland. This chapter provides a short overview of CERN and its accelerators, the LHC, as well as a short description of the main components of the CMS experiment.

3.1 The Large Hadron Collider

The LHC [1] is currently by far the largest and most powerful particle accelerator in the world. It is a circular accelerator situated in a tunnel around 100 metres below the Swiss-French border west of Geneva. Its main purpose is accelerating protons to energies of up to 13 TeV [1] in the final development stage of the machine starting in 2015. Besides the acceleration of protons it is also capable of accelerating heavy ions (predominantly lead ions) to energies of up to 2.76 TeV per nucleon.

3.1.1 The acceleration chain

Particles injected into the LHC for final acceleration are required to have an energy of 450 GeV. This is achieved by a long chain of linear and circular accelerators, a sketch of which can be seen in Fig. 3.1.

Protons used for acceleration in the LHC are extracted from a hydrogen molecules in a bottle situated at the CERN main site. These molecules are stripped of their electrons

[1] One electronvolt (eV) is the energy acquired by a charge of $1e$ passing through an electric field of 1 volt, equivalent to 1.602×10^{-19} Joule.

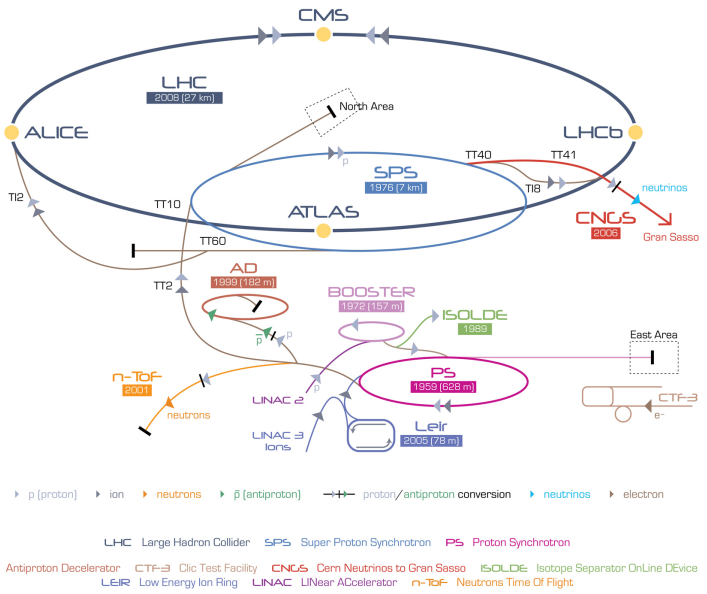

FIGURE 3.1: Conceptual drawing of all accelerators and experiments hosted at CERN. Besides operating the LHC, there are many other accelerators, decelerators and experiments being operated.

by strong electric fields and subsequently injected into the first acceleration stage, the linear accelerator Linac 2. Upon exiting Linac 2, the protons have gained an energy of 50 MeV and are injected into the first circular accelerator, the Booster. This synchrotron with a circumference of 157 meters accelerates the protons to an energy of 1.4 GeV and uses magnetic dipole fields to bend the protons onto a circular path. These bending magnets are operated at room temperature for the Booster and in fact all the accelerators up to the LHC. From the Booster, the protons are injected further into the Proton Synchrotron, an accelerator originally built in 1959 with a circumference of 628 meters and an output energy of 25 GeV. The last step before injection into the LHC is the Super Proton Synchrotron (SPS), which accelerates the protons to the LHC injection energy of 450 GeV. The SPS is the world's second largest accelerator with a circumference of nearly 7 km, and it was the first accelerator to collide protons and anti-protons at energies high enough to produce W and Z bosons, leading to their discovery in 1983 [2, 3].

Ions pass through the same accelerators on their way to the LHC with the notable exception of the very first acceleration being done in Linac 3 rather than Linac 2.

While the LHC is filled and delivering collisions to its experiments, the accelerators are used to provide particles to other experiments ongoing at CERN. The Antiproton Decelerator (AD) in which anti-protons are decelerated and combined with positrons to form anti-hydrogen, and the ISOLDE collaboration for the study of many different radioactive ions are just some of the examples of interesting experiments ongoing at CERN.

3.1.2 Specifications of the LHC

The LHC itself is located in a tunnel roughly 50-150 meters below ground in the Geneva area, extending from Lake Geneva all the way to the Jura mountain chain. Its total circumference is 26 659 meters which makes it – together with its predecessor the Large Electron Positron Collider hosted in the same tunnel – by far the largest particle accelerator ever built. It is divided into 8 sectors, separated and named by the eight access points to the tunnel. A schematic drawing of the LHC with all its access points can be found in Fig. 3.2. Access points 1, 2, 5, and 8 host the four main experiments ATLAS, ALICE, CMS, and LHCb, the acceleration is performed by radio-frequency (RF) cavities at point 4, the beam-dump system is located at point 6 and beam monitoring and conditioning is performed at points 3 and 7 [4].

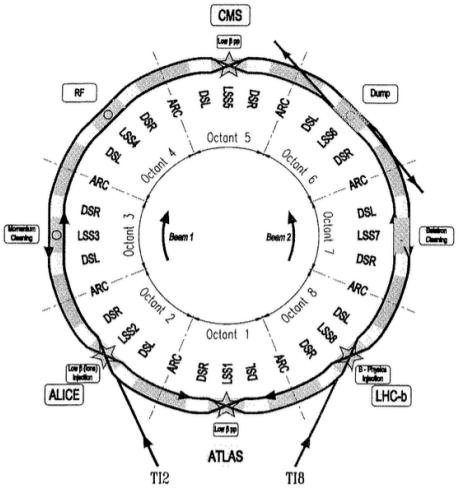

FIGURE 3.2: Schematic drawing of the LHC ring and its sectors and access points numbered in clockwise direction starting at the ATLAS experiment in point 1.

The magnet system

Particles are injected from the SPS into the LHC into two counter-rotating beams in discrete bunches at the aforementioned 450 GeV. In order to control the particles on their circular path, an intricate magnet system was designed in order to bend and to focus the beams. The main feature of the LHC magnet system are the 1232 dipole bending magnets, each roughly 15 meters in length and weighing 30 tonnes. These magnets are made of a niobium-titanium alloy, a type-2 superconductor which allows current transport without loss at the operating temperature of 1.9 K. Cooling of the LHC cold mass of roughly 37 Mt is achieved with pressurized superfluid helium. Each magnet hosts two separate beam-pipes for beam 1 (clockwise) and beam 2 (counter-clockwise)

with the dipole magnetic field pointing in opposite direction in either of them. In order to achieve acceptable beam lifetimes and to minimize beam-gas interactions, the beam pipes are evacuated and the residual gas pressure is around 10^{-10} mbar. Upon injection from the SPS the dipole magnets are operated at a magnetic field strength of 0.535 T which is slowly raised during the acceleration period of the beam to a final field strength of 8.33 T at the maximum collision energy.

Alongside the dipole magnets for the bending of the particles, there are thousands of additional magnets for correcting and controlling the particle's path. The largest part of the correction magnets are sextupole magnets situated on either side of every dipole magnet. Further components include a decapole and an octupole corrector for each dipole magnet as well as injection kicker magnets and kicker magnets for the beam dump system among others.

The RF cavities

Once the LHC is filled and circulation of the beams is stable, they are accelerated from their initial energy by the means of so-called RF cavities which provide a high frequency alternating electric field of nominally 400.8 MHz. Similar to the bending magnets, the RF cavities are operated in a superconducting state at a temperature of 1.9 K. There are a total of eight such cavities per beam, each achieving a potential difference of 2 MV for a combined 16 MV necessary for acceleration at collision energy. During the acceleration period of the beams, the energy gain per particle per turn is 485 keV with the total power consumption of the RF system being around 275 kW.

Beam parameters

In order to measure the performance of a particle accelerator such as the LHC, the quantities of instantaneous and integrated luminosity are the most important figure of merit, as they correspond to the total number of particle collisions produced in any given collision point. The instantaneous luminosity is defined as

$$L = \frac{N_b^2 n_b f_{rev} \gamma_r}{4\pi \epsilon_n \beta^*} F, \tag{3.1}$$

where N_b denotes the number of particles per bunch, n_b the number of bunches per beam, f_{rev} the revolution frequency of each bunch, γ_r the relativistic gamma factor, ϵ_n the normalized beam emittance, β^* the β-function of the beam at the collision point, and

TABLE 3.1: Beam parameters for beams in the LHC at injection and collision energy.

Beam parameters			
	Unit	Injection	Collision
Beam Energy	[GeV]	450	3500 - 7000
Relativistic γ_r		479.6	3730-7461
Particles per bunch		1.15×10^{11}	
No. of bunches		2808	
f_{rev}	[Hz]	11245	
ϵ_n	[μm rad]	3.5	3.75
Half crossing angle[2]	[μrad]	$\pm$ 160	$\pm$ 142.5
β^*	[m]	18	0.55

F a geometrical factor inversely proportional to the crossing angle of the two beams at the interaction point.

The beam emittance is defined as the volume of the beam in the position-momentum phase space and is thus a measure of the quality of the beam. Emittance itself is inversely proportional to the beam momentum and it is therefore necessary to introduce a normalized emittance, which does not change its value with momentum in order to compare beam quality before and after acceleration. The β-function describes the behavior of the transverse beam size as a function of the position in the accelerator, and the value β^* is consequently proportional to the transverse size of the beam at the collision point.

The dimension of the instantaneous luminosity is $cm^{-2}s^{-1}$ and by integrating it over time the integrated luminosity $\mathcal{L}_{int}$ is obtained. Through knowledge of the latter, one can calculate the total number of expected events for any given physical process in a data sample of a given size by

$$N_{\text{process}} = \mathcal{L}_{int} \cdot \sigma_{\text{process}}. \tag{3.2}$$

All relevant beam parameters to calculate the instantaneous luminosity at the LHC are summarized in Table 3.1 at both injection and collision energies.

Performance of the LHC

All values in Table 3.1 refer to the design values of the LHC, while the actual performance since startup in 2008 has been considerably different. After the initial startup in the autumn of 2008 when beams were first injected into the machine, a faulty connector between superconductors caused a significant explosion in the cooling system of the

main magnets, resulting in a shutdown and repair period until late 2009. However, upon restarting of the machine in 2009, operations of the LHC have been almost flawless, with many parameters of the LHC reaching or even exceeding their design targets. Since the limiting factor for the LHC energy is the attainable magnetic field strength in the bending magnet, combined with safety concerns regarding the replaced connectors from the incident in 2008, a staged approach for a slow energy ramp-up was implemented for the LHC. First stable collisions for data-taking in 2010 were performed at an energy per proton of 3.5 TeV resulting in 7 TeV center-of-mass energy. This energy was maintained also during 2011 before being increased to 8 TeV in center-of-mass energy during the 2012 data-taking period. This thesis focuses on the dataset at 8 TeV. The energy will further be increased to 13 TeV in center-of-mass in early 2015.

Regarding the luminosity, the LHC has outperformed its early expectations. Despite the fact that so far only half the bunches were filled, resulting in a bunch spacing of 50 ns instead of the design 25 ns, the maximum instantaneous luminosity has almost reached its design value of $1 \times 10^{34}\ cm^{-2}s^{-1}$ in late 2012, when an LHC fill with an instantaneous luminosity of $7.67 \times 10^{33}\ cm^{-2}s^{-1}$ was recorded. This was mostly due to the increase in protons per bunch.

Pileup

In order to reach the luminosities discussed in the previous section, it is necessary for the LHC to produce more than one proton-proton collision per bunch crossing in the experiments. This effect is called pileup and poses great difficulty to the experiments in handling multiple interaction vertices. Some problems include the identification of the 'interesting' vertex, the assignment of electrically neutral particles to said vertex, energy corrections for detector objects such as jets, leptons, and the missing momentum due to pileup interactions, and occupancy in the subdetectors. The number of proton-proton interactions per bunch crossing follow a Poisson-distribution of which the mean was about FIXME in 2010, and about FIXME in 2012, with the values of 2011 lying in between.

3.2 The CMS experiment

As briefly mentioned before, the LHC provides high energy particle collisions to four large particle physics experiments, namely the ALICE, ATLAS, CMS, and LHCb experiments. While the ALICE and LHCb experiments are specially designed for specific

purposes, the study of heavy ion collisions and the study of processes involving the b-quark, respectively, the ATLAS and CMS experiments are design as 'general purpose' experiments. As such, their goal is the detailed scrutiny of the SM, the search for the recently observed Higgs boson [FIXME - reference], and the search for new physics phenomena. They do this by means of measuring and absorbing decay products of the collisions. The relevant physical observables of any particle produced in a particle collisions are the momentum vector and the energy of a particle. Once these two quantities are known, every particle can be identified unambiguously.

Data collected for this thesis were recorded by the CMS experiment.

3.2.1 General structure and the magnet

The Compact Muon Solenoid (CMS) experiment is located roughly 100 meters below ground in Cessy, France, it is cylindrically shaped with dimensions of roughly 22 meters in length and a diameter of about 16 meters. The whole apparatus comprises a barrel part in the center and a so-called endcap on either side to seal the detector as hermetically as possible. A drawing of the CMS detector is shown in Fig. 3.3.

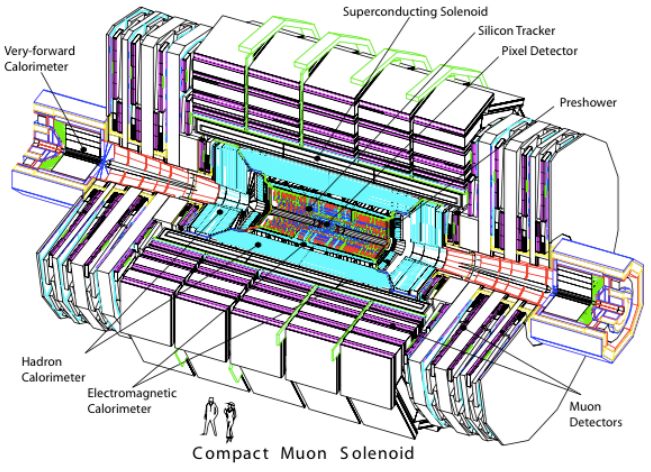

FIGURE 3.3: Perspective view of the CMS detector. The cylindrical shape as well as the barrel and endcap geometry can be clearly seen. The depicted people are to scale [4].

The convention for the coordinate system is as follows. The origin of the coordinate system is at the nominal interaction point. The x-axis points towards the center of the LHC ring, the y-axis points towards the surface and the z-axis points towards the

west, along beam 2. The azimuthal angle ϕ is measured in the x-y plane, while the polar angle θ is measured from the positive z-direction. It is commonly replaced by a quantity called pseudo-rapidity defined as $\eta = -\log\left[\tan\left(\frac{\theta}{2}\right)\right]$.

As the presence of the word 'solenoid' in the acronym for CMS already suggests, its main feature is a very large, solenoid magnet which defines the overall structure of the experiment. Much like the LHC bending magnets, it is a superconducting structure and the conducting material is a niobium-titanium alloy, albeit at a very different scale. It measures roughly six meters in inner diameter and 13 meters in length, carrying a current of about 18 000 (FIXME) ampere, resulting in a maximum magnetic field strength of 3.8 T [5]. In addition to the actual magnet, the CMS magnet system also comprises a return yoke for the magnetic field lines to be homogeneous as a function of the distance from the interaction point. Altogether, the magnet system weighs approximately 11 000 metric tons, by far the heaviest component of the CMS detector. As momentum resolution of charged particles is a critical factor in the physics performance of a detector, the magnetic field strength within the tracking volume is desired to be as large as possible.

The large volume of the CMS magnet allows for most sub-detectors to be situated within a very high magnetic field. Not only the tracking detectors, but also the calorimetry for energy measurement are fully incorporated within the magnet's volume.

3.2.2 The sub-detectors

The structure of CMS is a layered, onion-like assembly of different sub-detectors. In the very center, the beryllium beam-pipe passes through the detector with a diameter of 2.5 cm FIXME!!. Moving radially outwards from the center of the beam-pipe, the layers are first the silicon pixel detector followed by the silicon strip tracker, the electromagnetic calorimeter, the hadronic calorimeter, the superconducting magnet and finally the magnet return yoke interleaved with the muon chambers.

The CMS pixel detector

The CMS pixel detector is a layered silicon detector with a pixel size of $100 \times 150\ \mu m^2$ with the purpose of measuring the trajectory of charged particles very precisely. It is divided into a barrel (BPIX) and two endcap 'forward' parts (FPIX) symmetrically arranged around the nominal interaction point. The BPIX comprises three concentrical layers of 53 cm in length and at radii of 4.3, 7.2, and 11 cm from the interaction point, while there are two FPIX disks on either side of the BPIX, at distances of z=$\pm$34.5 and z=$\pm$46.5 cm, extending from a radius of 6 to 15 cm. In combination, the barrel and

endcap part provide high granularity tracking up to a pseudo-rapidity of $\eta = 2.5$, corresponding to a polar angle of roughly 10°. A sketch of both the pixel detector and the silicon strip can be found in Fig. 3.4.

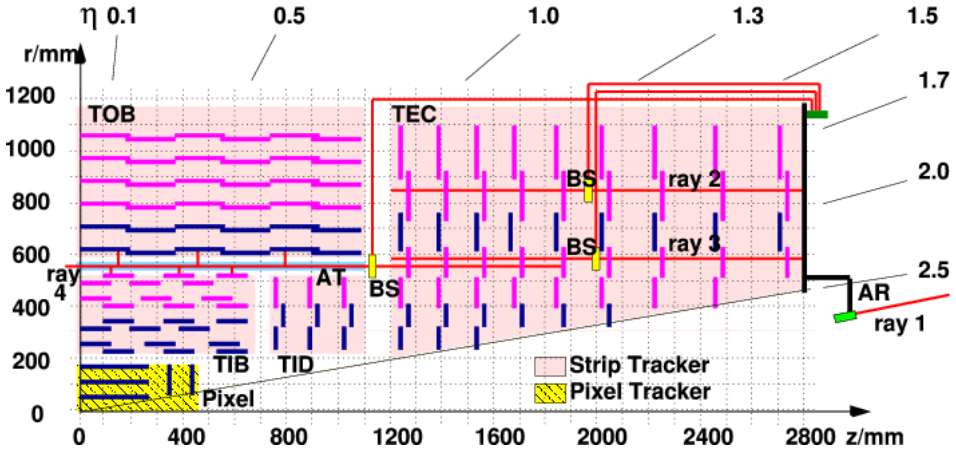

FIGURE 3.4: Sketch of a quarter of all parts in the CMS tracking system with distances in radius r and z. The pixel detector is close to the interaction point shown in yellow, the silicon strip tracker is underlaid in pink. Each pink and blue solid line represents an active detector layer [6].

Both the FPIX and the BPIX are organized into single detector modules. There are 768 modules in the barrel part and 672 modules in the four forward disks, each consisting of 2 to 16 readout chips (ROCs) [7]. Every ROC has a size of roughly 8×8 mm^2 and is bump-bonded to an active silicon layer of 285 µm in thickness, divided into 52×80 single pixels. In total, there are 1440 modules containing about 16 000 ROCs with a gross pixel count of about 66 million and a total silicon area of about one square meter. Such a high granularity is needed in order to obtain good spacial resolution at the interaction point, good reconstruction of the tracks and in order to keep the occupancy low in high luminosity running of the LHC. At design luminosity of 1×10^{34} m^{-2} s^{-1}, the CMS pixel detector is hit by about 1000 particles per bunch crossing, leading to an occupancy of less than one percent. Even with relatively low occupancies, the total flux of particles in the inner layers of the pixel detector are sufficiently high to induce significant radiation damage. For this reason, the pixel detector has to be replaced during run 2 of the LHC, an event scheduled for late 2017.

The silicon strip tracker

Just outside the pixel detector, further away from the interaction point lies the silicon strip tracker. Its purpose is much the same as the pixel detector, albeit with a much larger covered area and a much smaller number of active channels. It occupies the radial distances from 20 to 116 cm and a length in z-direction of 5 8 m. It is also divided

into a cylindrical barrel part and endcap parts perpendicular to the beam direction. The naming scheme of the different parts is the Tracker Inner Barrel (TIB) and the Tracker Outer Barrel (TOB) for the layers parallel to the beam direction and the Tracker Inner Disks (TID) and the Tracker EndCaps (TEC) for the perpendicular part. In total, there are 15 148 single detector modules in the silicon strip tracker[8] with varying sizes of strip widths and inter-strip pitch lengths. The inter strip pitch varies from 80 µm at low radius to 200 µm at higher radius, while the ratio between pitch and width is constant at 0.25. The combined surface of the 9.3 million single channels is around 198 m^2, making it the largest silicon tracker ever built. The thickness of the silicon also varies between 320 µm in the inner part of the detector and 500 µm on the outside part. With this specifications, the total occupancy at design luminosity is approximately 1%. Altogether, a particle traversing the strip tracker will hit about ten active silicon layers[3].

Due to the high granularity, the multi-layered design, and the very high and homogeneous magnetic field in the tracking volume, the performance of the CMS tracking system is impressive. Single point resolutions are around 30 µm and in combination, the impact parameter resolution of is around around 10 µm for high energy muons, while the momentum resolution varies from around 1% for low-p_T muons in the central region to about 8% for high-p_T muons in the forward region.

The electromagnetic calorimeter

CMS has adapted a design with two separate calorimeters for electromagnetically and hadronically interacting particles. Both of those calorimeters are contained within the superconducting magnet, as shown in a sketch of the CMS calorimetry in Fig. 3.5.

The electromagnetic calorimeter (ECAL) is a homogeneous calorimeter made of 68 524 lead tungstate ($PbWO_3$) crystals built to absorb and measure electromagnetically interacting particles such as photons and electrons. The material was chosen for its mechanical and scintillating properties. With a density of 8.28 $kg\,m^{-3}$ it has a very short radiation length of 0.89 cm as well as a small Molière radius of about 2.2 cm[4] , allowing for a high granularity and adequate spacial resolution of electromagnetic showers. Its scintillating properties include a very short signal collection time of about 25 ns for 80% of the signal and a relatively low photo-electron output of 4.5 per MeV in a wavelength spectrum with a broad maximum in the blue-green 420-430 nm region. This light is collected and amplified by photo-multipliers which are mounted to the rear end of the

[3]This depends on the exact trajectory and varies between eight and 14 layers.

[4]The radiation length is the distance at which the energy of an incoming electron has decreased to $\frac{1}{e}$ ∼37% due to bremsstrahlung and about $\frac{7}{9}$ times the distance after which a high energy photon would produce an e^+e^- pair. The Molière radius defines the transverse containment of an electromagnetic shower.

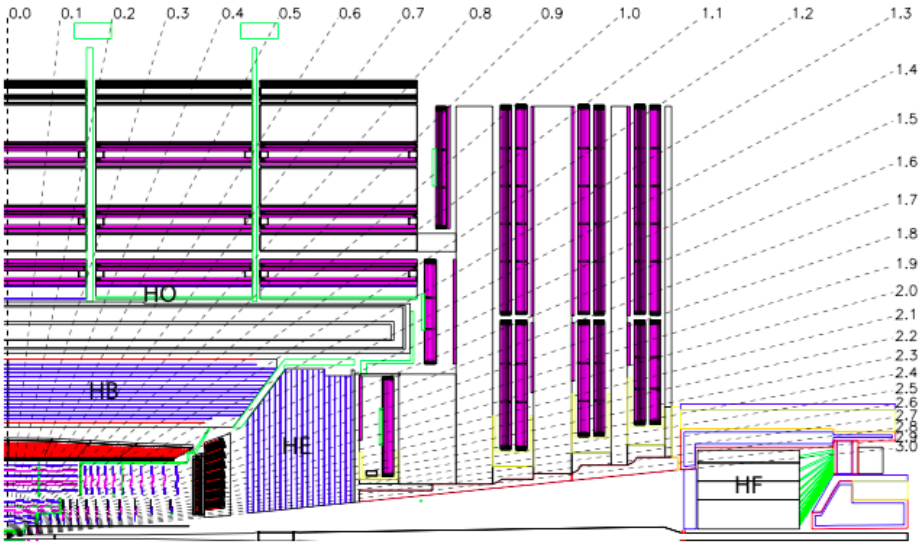

FIGURE 3.5: Design of the CMS calorimetry system. The homogeneous electromagnetic calorimeter is shown in red towards the center of the detector, while the hadronic calorimeter extends to larger radii [4].

crystals. Each crystal has an area of 22×22 mm^2 on the front facing side and 26×26 mm^2 on the far side, corresponding to a spacial resolution of 0.0174×0.0174 in η-ϕ. The length in radial direction is 230 mm, corresponding to 25.8 radiation lengths. The barrel part of the ECAL (EB) extends to $|\eta| = 1.479$, and the endcap part (EE) covers the pseudorapidity range from $1.479 < |\eta| < 3.0$.

The energy resolution of a calorimeter can be parametrized by

$$\left(\frac{\sigma}{E}\right) = \left(\frac{\mathrm{a}}{\sqrt{E}}\right) \oplus \left(\frac{\mathrm{b}}{E}\right) \oplus \mathrm{c}, \tag{3.3}$$

where a is called the stochastic term, b the noise term, and c a constant term. At low particle energies both the stochastic term and the noise term dominate the resolution, while at higher energies the importance of the constant term becomes more important. From measurements in testbeams, the terms for the energy resolution of the CMS ECAL were found to be

$$a = 2.8\%,$$
$$b = 12.0\%,$$
$$c = 0.3\%,$$

[9] for the energy in GeV . For the most relevant physical processes, such as $H \to \gamma\gamma$ or $Z \to e^+e^-$, the total resolution both for electrons and photons is of the order of 1% in the central part and of the order of a few percent in the forward part of the detector.

The hadronic calorimeter

For an accurate measurement of the missing transverse energy or momentum, a precise knowledge of the energy of hadronic jets is of paramount importance. However, since the available volume within the CMS magnet is limited, a compromise on the hadronic calorimeter (HCAL) had to be made. The implemented design is a sampling calorimeter, interleaved layers of a massive passive absorber material and a lighter, but active scintillating material. The task of the passive absorber is to create particle showers, which can then be measured in the active material.

The geometry is again divided into a barrel (HB) and an endcap (HE) part. The HB consists of two steel plates as first and last absorber layer and 14 layers of brass of variable thickness in between. In total, these 16 layers of absorber material in the barrel amount to 5.82 interaction lengths [5] of material at $\eta = 0$ up to 10.6 interaction lengths at $|\eta| = 1.3$. The HE is composed of 18 brass absorber plates constituting about 10 interaction lengths along the coverage up to $|\eta| = 3.0$. Every absorber plate is combined with a layer of plastic scintillator organized in tiles each occupying an area of 0.087×0.087, which drives the spacial resolution of the hadronic calorimeter. In addition to the components contained within the superconducting magnet, the hadronic calorimeter features another layer of detector material just outside the magnet, called the hadronic outer (HO) in order to measure hadronic jets with an energy sufficient to traverse the HB and the magnet (so-called punch-throughs). There is also a hadronic calorimeter for high-η jets, called the hadronic forward (HF) covering pseudo-rapidities of $3.0 < |\eta| < 5.0$.

Since the HCAL is a sampling, rather than a homogeneous, calorimeter involving large parts of inactive material, its energy resolution is significantly worse than the one of the ECAL. Adding to this lower precision is the fact that hadronic interactions are accompanied by some unmeasurable energy losses in nuclear excitations. Using the same parametrization as in Eq. 3.3, the parameters for the HCAL are found to be

$$a = 1.25,$$
$$b = 5.6,$$
$$c = 0.033.$$

For relevant hadronic jets in analyses for SUSY and most other use-cases, the resolution takes values of about 25 % for 40 GeV jets and decreases with energy to values of about 10 % or less at energies of jets above 100 GeV.

[5] An interaction length corresponds to the mean distance at which a hadronic particle undergoes a nuclear interaction.

The muon system

As the acronym CMS already suggests, special emphasis in the design of the detector was put into designing and constructing a system which is capable of measuring muons with a very high precision in order to be sensitive to high-sensitivity processes such as the Higgs boson decaying into four leptons. This is achieved by three types of gaseous detectors encased in the return yoke of the magnet, namely the Drift Tubes (DTs) in the barrel part, Cathode Strip Chambers (CSCs) in the two endcap parts, and a set of fast Resistive Plate Chambers (RPCs) used for triggering on muons and timing. The total coverage can be expressed by the reconstruction efficiency as a function of the pseudo-rapidity, which achieves values close to 100 % all from values of $0. < |\eta| < 245$, with a notable exception at around $|\eta| = 0.25$, and $|\eta| = 0.8$, where it drops to around 94 % and 97 %, respectively, due to small gaps between the DTs. The layout of the muon system can be seen in Fig. 3.6, where a quadrant of the CMS detector is shown.

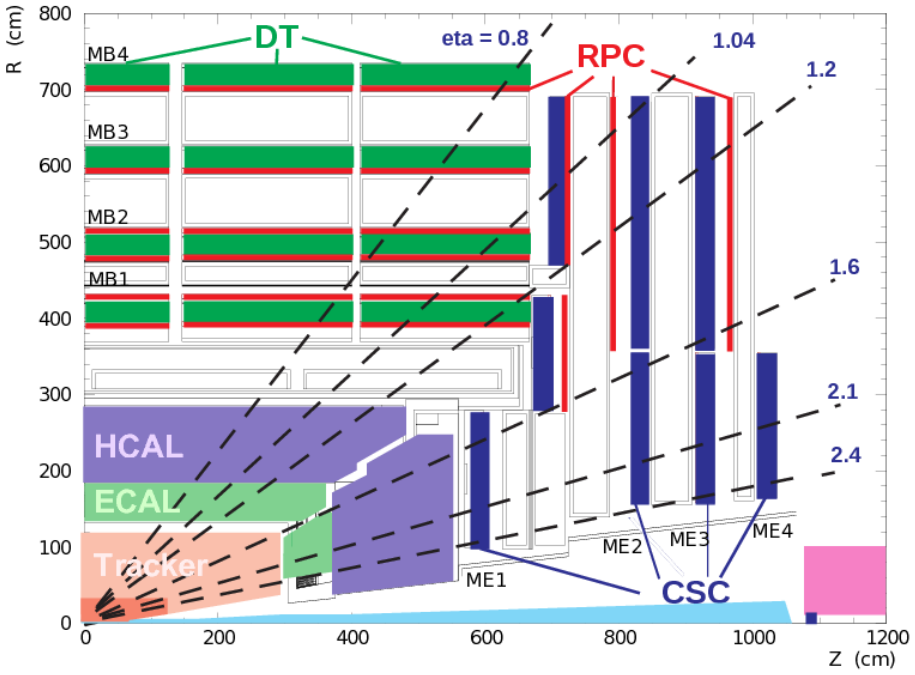

FIGURE 3.6: Layout of the CMS muon system. The DTs comprise the barrel part of the detector, while the CSCs are exclusively situated in the endcap part. RPCs are attached to both types of detectors for triggering and timing measurements [10].

The DTs are organized in four concentrical cylinders in the barrel part with a total of 250 drift chambers containing 172 000 active wires. They are made of multiple so-called superlayers, which are essentially stacked tubes either in beam direction or perpendicular to it. Two or three of those superlayers are then combined into one DT, with altering orientation of the wires to provide maximum spacial resolution. RPCs are glued to the DTs, on both sides for the inner two cylinders and on the inner side for the outer two.

The gas in the drift tubes is a mixture of 85% Ar and 15% CO_2 and the drift length is chosen to be 21 mm with a drift time of roughly 380 ns, allowing for negligible occupancy.

Because of the much higher flux and an inhomogeneous magnetic field in the forward part of the detector, a different detector design had to be chosen for high values of $|\eta|$. The CSCs are a set of 468 trapezoidal modules, each covering from 10° to 20° in ϕ. Each CSC consists of six gas-filled gaps with cathode strips running radially and anode wires running almost perpendicular to the strips. The r, ϕ, and z coordinates of a traversing muon is thus measured six times per CSC, and there are in total four layers of CSCs in each endcap. There are a total of 220 000 readout channels of the strips and another 180 000 readout channels of the wires, allowing for good spacial resolution and low occupancy even at high flux rates of up to 1 kHz cm^{-2} at full LHC luminosity. The gas mixture is 40% Ar, 50% CO_2, and 10% CF_4, where the CO_2 component achieves a high signal gain, while the CF_4 component protects the wires from polymerisation. Three layers of RPCs are connected to the CSCs in the outer part of the endcap.

RPCs are gas-filled detectors which have a very fast signal rise-time, comparable to that of scintillators. Since the time resolution is much better than the LHC bunch spacing of 25 ns, the RPCs provide not only an accurate estimate of the momentum of a muon, but also unambiguous assignment to a bunch crossing. Each RPC is made up of two 2 mm wide, gas-filled gaps with strips on the common side and plates of plastic on the outer sides. These simple circuits are operated in avalanche mode in order to ensure good operation at high rates.

Using the three muon-subsystems and combining their measurement, a standalone muon momentum resolution of below 10% can be achieved for muons up to 200 GeV. This value increases to between 15% and 40% for muons of 1 TeV momentum, depending on the position in $|\eta|$. Since a muon can be identified also in the tracker volume, combining the tracks from the inner part of the detector with the information of the muon chambers improves this resolution to roughly a percent for momenta below 200 GeV and about 5% for momenta of 1 TeV.

3.2.3 The trigger system

With a bunch crossing frequency of 40 MHz and a mean number of collisions per bunch crossing of roughly 20, there are up to 800 million collisions taking place inside CMS every second. Considering that the whole of CMS has roughly 100 million readout channels, this would lead to unsustainable data-rates, even for the most powerful readout

and network possible to date. For this reason, a triggering system has been implemented in order to differentiate 'interesting' collisions from those who are considered not. CMS has adopted a two-stage approach, with a first, hardware-based and thus very fast triggering mechanism called the Level-1 trigger (L1), followed by a second, fully software based trigger named the High-Level-Trigger (HLT).

The L1 trigger

Dealing with complicated data at a rate of 40 MHz requires for processing of information at speeds that are unattainable for software reconstruction. Therefore, a fully hardware based system has been implemented, relying heavily on the use of integrated circuits in the form of so-called Field-Programmable-Gate-Arrays (FPGAs). Because speed is such an important point of the triggering decision, not all information from the detector can be used in order to make a yes/no decision on an event-by-event basis. In the current L1 trigger system, only coarsly segmented information from the calorimeters and the muon system are used for the trigger decision, while the full data from the muon system, the calorimeter, and the silicon tracker are stored in buffers until a trigger accept (L1 accept) triggers the full readout of these buffers. An organizational sketch of the different participants for a trigger decision is shown in Fig. 3.7 The calorimeter

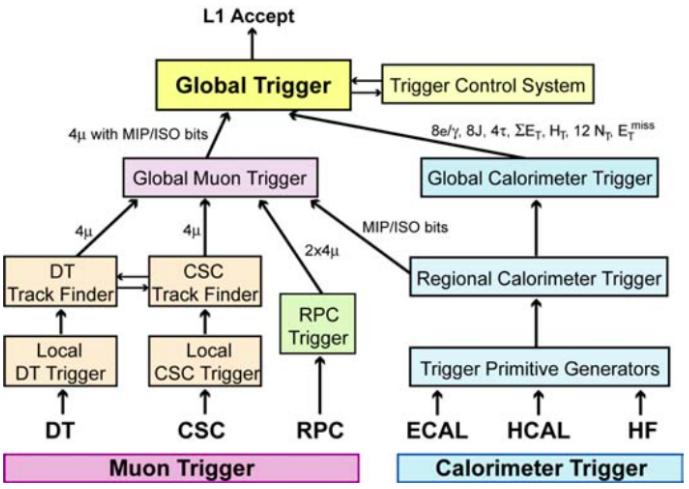

FIGURE 3.7: Organizational chart of the various components of any L1-accept. The two systems (calorimetry and muons) work in parallel until they are combined at a regional/global level into the global trigger decision [4].

part of the trigger has inputs from the ECAL, HCAL, and the HF, constructing first so-called Trigger Primitives from coarsly organized trigger 'towers'. These are then fed into a regional trigger, where energy sums and crude identifications of physical objects are performed. This information is then given to the global trigger, which constructs

relevant variables such as the total energy deposited, the number of jets, etc. In parallel, the muon system tries to identify tracks of muons and calculate their p_T .

The HLT

3.2.4 Reconstruction and data formats

3.2.5 Simulation and Monte-Carlo

Chapter 4

Same-sign dilepton analyses

4.1 Search for Supersymmetry in events with hadronic activity

4.2 Search for electroweak production of Supersymmetry

4.3 Fake leptons

Chapter 5

Outlook

Chapter 6

Conclusions

Appendix A

Dummy Appendix

You can defer lengthy calculations that would otherwise only interrupt the flow of your thesis to an appendix.

List of Figures

List of Tables

Abbreviations

LAH **L**ist **A**bbreviations **H**ere

Physical Constants

$$\text{Speed of Light} \quad c \quad = \quad 2.997\,924\,58 \times 10^{8}\ \text{ms}^{-\text{S}}\ \text{(exact)}$$

Symbols

a	distance	m
P	power	W (Js^{-1})
ω	angular frequency	$rads^{-1}$

Bibliography

[1] Oliver Sim Brüning, Paul Collier, P Lebrun, Stephen Myers, Ranko Ostojic, John Poole, and Paul Proudlock. *LHC Design Report*. CERN, Geneva, 2004.

[2] The UA1 collaboration. *Experimental observation of isolated large transverse energy electrons with associated missing energy at s=540 GeV*. *Physics Letters B*, 122(1):103 – 116, 1983. ISSN 0370-2693. doi: http://dx.doi.org/10.1016/0370-2693(83)91177-2. URL http://www.sciencedirect.com/science/article/pii/0370269383911772.

[3] The UA1 collaboration. *Experimental observation of lepton pairs of invariant mass around 95 GeV/c^2 at the CERN SPS collider*. *Physics Letters B*, 126(5):398 – 410, 1983. ISSN 0370-2693. doi: http://dx.doi.org/10.1016/0370-2693(83)90188-0. URL http://www.sciencedirect.com/science/article/pii/0370269383901880.

[4] R. Adolphi et al. The CMS experiment at the CERN LHC. *JINST*, 3:S08004, 2008. doi: 10.1088/1748-0221/3/08/S08004.

[5] *The CMS magnet project: Technical Design Report*. Technical Design Report CMS. CERN, Geneva, 1997.

[6] W. Adam et al. Alignment of the CMS Silicon Strip Tracker during stand-alone Commissioning. *JINST*, 4:T07001, 2009. doi: 10.1088/1748-0221/4/07/T07001.

[7] D. Kotliński, E. Bartz, W. Erdmann, K. Gabathuler, R. Horisberger, Ch. Hörmann, H-Ch. Kästli, B. Meier, and S. Schnetzer. The control and readout systems of the CMS pixel barrel detector. *Nuclear Instruments and Methods in Physics Research Section A: Accelerators, Spectrometers, Detectors and Associated Equipment*, 565(1):73 – 78, 2006. ISSN 0168-9002. doi: http://dx.doi.org/10.1016/j.nima.2006.04.065. URL http://www.sciencedirect.com/science/article/pii/

S0168900206007200. Proceedings of the International Workshop on Semiconductor Pixel Detectors for Particles and Imaging PIXEL 2005 International Workshop on Semiconductor Pixel Detectors for Particles and Imaging.

[8] Paolo Azzurri. The CMS silicon strip tracker. *J.Phys.Conf.Ser.*, 41:127–134, 2006. doi: 10.1088/1742-6596/41/1/011.

[9] The CMS Collaboration. Energy calibration and resolution of the CMS electromagnetic calorimeter in pp collisions at $\sqrt{s}$ = 7 TeV. *Journal of Instrumentation*, 8 (09):P09009, 2013. URL http://stacks.iop.org/1748-0221/8/i=09/a=P09009.

[10] Min Suk Kim et al. CMS reconstruction improvement for the muon tracking by the RPC chambers. *PoS*, RPC2012:045, 2012. doi: 10.1088/1748-0221/8/03/T03001.